Journal of Physics: Conference Series **1559** (2020) 012061 doi:10.1088/1742-6596/1559/1/012061

# The Comparative Study of the Internal Tin $Nb_3Sn$ Wires with Different Layouts

**P A Lukyanov[1], V I Pantsyrny[1,2], M V Polikarpova[1], V V Guryev[1], D S Novosilova[1], K O Bazaleeva[1], A S Tsapleva[1], M V Alekseev[1], A G Silaev[1], I M Abdyukhanov[1], V V Sergeev[2]**

[1] - Bochvar Institute (VNIINM), Moscow, Russia
[2] - Research and Production Company "NANOÉLECTRO", Moscow, Russia

pallukyanov@bochvar.ru

**Abstract**. The required combination of performance properties for internal tin $Nb_3Sn$ wires for high energy physics includes high critical current density ($J_c$) and RRR values as well as low magnetization and effective diameters ($D_{eff}$) value. It is quite a challenge to achieve them all at once. A comprehensive study has been carried out on two internal tin $Nb_3Sn$ wires with essentially different layouts and 37 sub-elements each. The first type of wires has distributed diffusion barriers. The second one has common diffusion barrier with sub-elements internally divided by resistive separators. Two sets of data for two types of wires have been obtained, which include transport measurements of $J_c(B)$, magnetization loops $M(B)$, superconducting transition temperature $(T_c)$, $RRR$ values, Sn-concentration by EDAX measurements and XRD analysis. XRD analysis of the superconducting layers has shown that the compressive macrostress is larger for the wire with overall barrier than for the wire with distributed diffusion barriers. This observation correlates with a shift of the stress-dependent curves of the superconducting transition. The difference in the volume fractions and the homogeneities of the $Nb_3Sn$ phase leads to a significant difference of the $J_c(B)$ dependences and the values of the Kramer critical field $(B_{Kr})$ for these types of wires. In summary, the high critical current density for the first type of wires and the low hysteresis losses for the second type of wires have achieved with high RRR values in both cases.

## 1. Introduction

$Nb_3Sn$ superconductors intended for magnetic system of particle accelerators must have a set of characteristics, which today is not implemented in the world. The main difficulty consists in simultaneously achieving an extremely high critical current density (the target is 1500 A / $mm^2$ at 16 T and 4.2 K) and a relatively small level of hysteresis losses, which are determined in the specification (table 1) by the effective diameter of superconducting filaments ($D_{eff}$ – 20 μm) [1].

**Table 1.** Target Characteristics of $Nb_3Sn$ Wires [1] for FCC project

| | | |
|---|---|---|
| Strand diameter | mm | 0.5….1 |
| Non-Cu $J_c$ (16 T, 4.2 K) | A/mm$^2$ | ≥1500 |
| $\mu_0\Delta M$ (1 T, 4,2 K) | mT | ≤150 |
| $\sigma(\mu_0\Delta M)$ (1 T, 4,2 K) | % | ≤4.5 |
| $D_{eff}$ | μm | ≤20 |
| RRR | – | ≥150 |
| Unit Length | km | ≥5 |

The set of characteristics given in the specification suggests the use of $Nb_3Sn$ wires obtained by the internal tin source (IT) method, since so far only conductors of this type have been demonstrated the possibility of reaching sufficiently high content of the superconducting phase.

To develop a cost-effective technology for the production of wires with the specified characteristics, CERN advanced a program in which more than 10 technological and research groups around the world participated [2]. In accordance with the program [2], the task of achieving the required properties is divided into stages. At the first stages the value $D_{eff}$≤60 μm, and the length of a piece of wire is not less than 100 meters must be demonstrated.

In Bochvar Institute (VNIINM) two wire designs were investigated in the framework of this program: wires with distributed and common barriers. The both approaches have been explored in VNIINM. The purpose of this paper is comparative study of $Nb_3Sn$ wires obtained by the internal tin source method of two fundamentally different designs and considering the advantages and disadvantages each of them

## 2. Materials and methods

Two sets of Internal Tin $Nb_3Sn$ wires with distributed and common diffusion barriers were designed in Bochvar Institute and fabricated in ChMP (Chepetsky Mechanical Plant). The cross-sections of wires are presented in Fig.1 and layouts of the wires are given in the table 2. To improve the deformability of the niobium barrier the Cu-Nb layer was introduce in the wire B around a common barrier. The wires A 1 mm in dia was produced in the long-length form and then tested in CERN [2]. During project development, the pilot wires (A and B) were deformed to 0.7 mm and studied in Bochvar Institute.

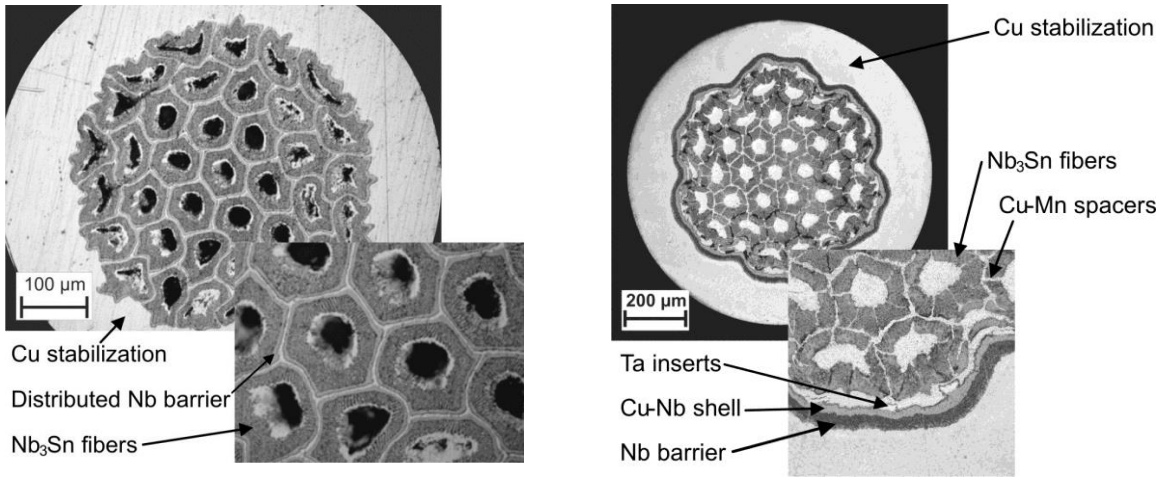


**Figure 1.** Cross sections of the reacted wires Ø0.7 mm and fragments (a) – wire A with distributed barrier and (b) - wire B with common barrier

**Table 2.** Layout of the wires

| Wire identification | A | B |
|---|---|---|
| Barrier | Distributed Nb | Common Nb+Ta |
| Wire dia, mm | 0.7 | 0.7 |
| Subelement number | 37 | 31 |
| Subelement size, μm | 80 | 70 |
| Clusters number | - | 31×6 |
| Resistive separator | - | Cu-Mn |
| Number of filaments | 29082 | 7988 |
| Filament diameter, μm | 1.6 | 3.5 |
| Nominal doping, at.%Ti | 1.4 | 2 |
| Cu/non Cu ratio | 1.3 | 1.2 |

Both types of wires were subjected to comprehensive study by means of various techniques. Transport critical current measurements ($I_c$) were carried out in accordance with IEC 61788-2 on the 1.5 m length wire mounted on the ITER-type mandrel in the fields range from 6 T to 12 T in a cryostat containing a superconducting 13 T magnet in the liquid helium bath (4.2 K). The current was ramped up at rates of up to 3 A/s and near the transition the ramp rate was reduced to less than 1 A/s. Thus the point density in transition curve was high enough. The critical current $I_c$ was evaluated using an electric field criterion $E_c$ of 10 μV× $m^{-1}$. The sample-to-rod contact resistance and the available cooling power in helium bath allows to achieve a current limit about 750 A. The critical current density ($J_c$) was determined by the cross-sectional area of the wire without copper. The *n*-values were evaluated from the power law portion of the E-I characteristic ($E = E_c(I/I_c)^n$).

The RRR-values and critical temperature measurements were done on the samples about 80 mm in length by the DC four probe technique with excitation current density not more than 1 A/$mm^2$ in order to keep the Joule heating reasonable. The temperature was measured by CX-1030-SD-4B Cernox thermometer placed near the sample.

Hysteresis losses were determined in accordance with IEC 61788-13 using a vibrating sample magnetometer with magnetic field amplitude up to ±5 T. Each sample coil form with 4-6 turns and outer diameter about 10 mm. The recording ramp rate |d*B*/d*t*| of hysteresis loop was 30 mT/s. The effective filament diameter, $D_{eff}$ , was estimated by a width magnetization loop at 3 T using equation [3]:

$$D_{eff}(B) = \frac{3\pi \cdot \Delta M}{4\mu_0 \cdot J_{ce}} \qquad (1)$$

where $\mu 0$ – vacuum permeability, $\Delta M$ – hysteresis loop width at 3 T, $J_{ce}$ – critical current density per total wire area taken at 3 T.

The Qualitative phase analysis was carried out on a D8 Advance (Bruker) X-ray diffractometer in Co-$K_\alpha$ radiation in the 2θ range 30–130° with a step of 0.07 degrees and an exposure of 1.5 sec at a point. To accurately determine the crystal lattice period of the $Nb_3Sn$ phase, reflection (321) was taken with a step of 0.02 degrees and exposure τ = 2 sec for samples of wires A and B and τ = 4 sec for sample A_powder. To determine the interplanar distance $d_{(321)}$, the reflection (321) for each trend was recorded twice with a remounting of the sample. The error in determining the lattice period was 0.0007 Å.

The superconducting phase inhomogeneity was determined by Energy-dispersive X-Ray (EDX) analysis.

For wires properties optimization a lot of reaction heat treatments were done mainly with last stage temperature at 665°C. It was found, that the optimal duration time of reaction at this temperature is not more than 50 hours for wire A and 100 hours for wire B.

## 3. Experimental results

### *3.1. The critical current measurements and $B_{Kr}$ evaluation*

The results of critical current measurements, $J_c$ and $B_{Kr}$ ($B_{c2}$ in the Kramer approximation) evaluations are presented in the table 3 and the figure 2.

**Table 3.** The $I_c$, $J_c$ (12 T, 4.2 K) values and $B_{Kr}$ estimation for investigated wires

| Sample | The last stage duration time at 665°C (hour) | Applied field (T) | $I_c$ (A) | n | $J_c$ (A/m | $B_{c2}$ (T) |
|---|---|---|---|---|---|---|
| Wire B | 100 | 12 | 238 | 22.6 | 1361 | 27.6 |
| | | 11 | 281 | 23.4 | 1607 | |
| | | 10 | 334 | 23.5 | 1910 | |
| | | 9 | 394 | 24.1 | 2253 | |
| | | 8 | 463 | 23.6 | 2648 | |
| | | 7 | 544 | 23.9 | 3111 | |
| | | 6 | 644 | 23.8 | 3683 | |
| Wire A | 50 | 12 | 429 | 32 | 2731 | 25.5 |
| | | 11.5 | 475 | 35 | 3024 | |
| | | 11 | 521 | 36 | 3317 | |
| | | 10.5 | 571 | 36 | 3635 | |
| | | 10 | 623 | 37 | 3966 | |
| | | 9.5 | 678 | 37 | 4316 | |

As the critical current measurements limit is about 750 A, only the measurements of wire A with diameter 0.7 mm were achievable, nevertheless the obtained $J_c$ results of wire A are in a good agreement with measurements of the wires 1 mm in dia in CERN [2].

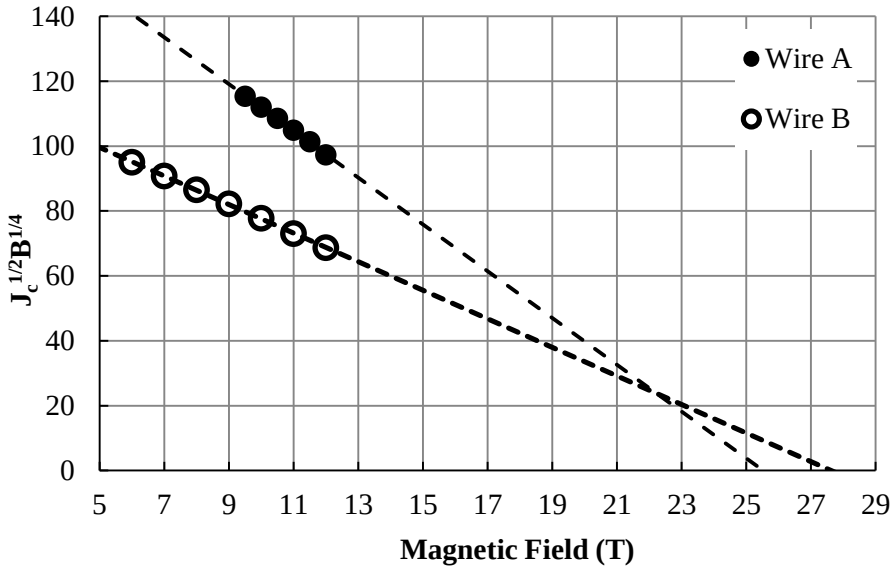


**Figure 2.** Kramer plot for wire A and wire B

The scaling critical fields ($B_{Kr}$) for 4.2 K determined from the linear Kramer extrapolation of the measured $J_c$ data are differ by 2 T (table 3). Such an increase in the critical field for wire B can be effects of composition and microstresses of superconducting layer. On the other hand extrapolated values of $J_c$ at 3 T more than 2 times higher for wire A.

*3.2. Magnetization and effective filament diameter*

In accordance of specification (table 1) a width of magnetization loop ($\Delta\mu_0 M$), referred to the sample volume must be less than 150 mT. The magnetization loops of both wires are presented in figure 3.

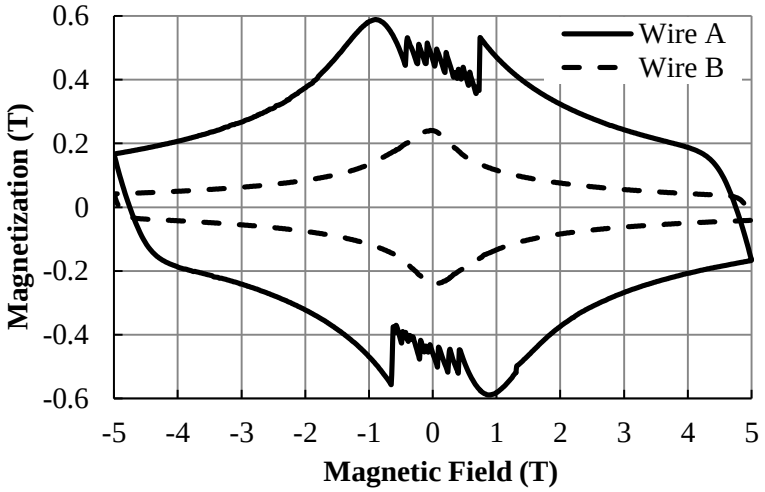


**Figure 3**. Hysteresis loops $M(B)$ for wire A and wire B

As can be seen there is qualitative difference between hysteresis loops of two wires. The wire A has pronounced jumps $M(B)$ in the range of fields up to ±1 T, while the wire B has an almost smooth $M(B)$ dependence. In accordance of the critical-state model the jumps indicate that eddy current at low fields exceeds critical value. The width of magnetization loop is much more than 150 mT for wire A, and its value meets specification for wire B.

The excess loss is determined by the proximity effect coupling and expressed by the $D_{eff}$ value. Based on the $\Delta M$(3 T) values the effective diameters values were evaluated in accordance with equation 1 and presented in the table 4.

**Table 4.** The results of $D_{eff}$ values determination

| Sample | Wire dia (mm) | Q (5T) (J×dm$^3$) | $D_{eff}$ (3T) (μm) | $D_{sub\text{-}element}$ (μm) |
|---|---|---|---|---|
| Wire A | 1.0 | 4 877 | 147 | 114 |
| Wire B | 1.0 | 1 340 | 70 | 103 |
| | 0.7 | 1 346 | 69 | 72 |

*3.3. Parameter RRR*

It is known, that the low RRR results of Internal Tin (IT) $Nb_3Sn$ wires with distributed barriers determined by tin diffusion through Nb barrier into copper matrix [4]. So optimization of geometrical parameters such as the barrier thickness and its continuity, copper volume fraction and its distribution are necessary for achieve RRR values in accordance with the specification (table 1).

The RRR measurements were performed on the wire with diameters of 1, 0.9 and 0.7 mm reacted with heat treatments at 665°C on the high temperature stage and various durations. As one can see from figure 4, the results of the RRR are affected both by reaction time and wire diameter. As it was stated in our earlier work [5], to provide an RRR level more than 150 the ultimate reaction time for wire A at the chosen reaction temperature should be not more than 50 hours for the wire 1 mm in dia.

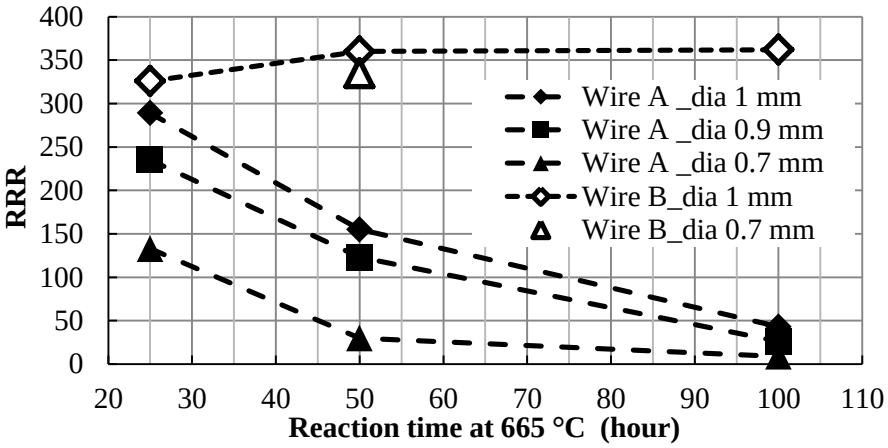


**Figure 4.** The RRR values of wire A and wire B with different diameters vs reaction time at 665°C

However the wire B has lower volume fraction of copper (table 2), its RRR values is almost independent on reaction time and wire diameter.

*3.4. Critical temperature*

The resistive transition of $Nb_3Sn$ wires is determined not only by the composition of the phase, its stressed state, but also by the resistance of the stabilizing copper, i.e. its volume fraction and the level of the parameter RRR. Therefore, the determination of the transition temperature should be performed on the samples after copper removal. Unfortunately, it is not possible to remove the entire copper component of the wire with a distributed barrier by etching while maintaining its integrity, therefore only the outer copper shell is removed. Wire B was measured both on samples without external copper and on the sample after removal of the niobium barrier and partial etching of the fibers (figure 5 and table 5).

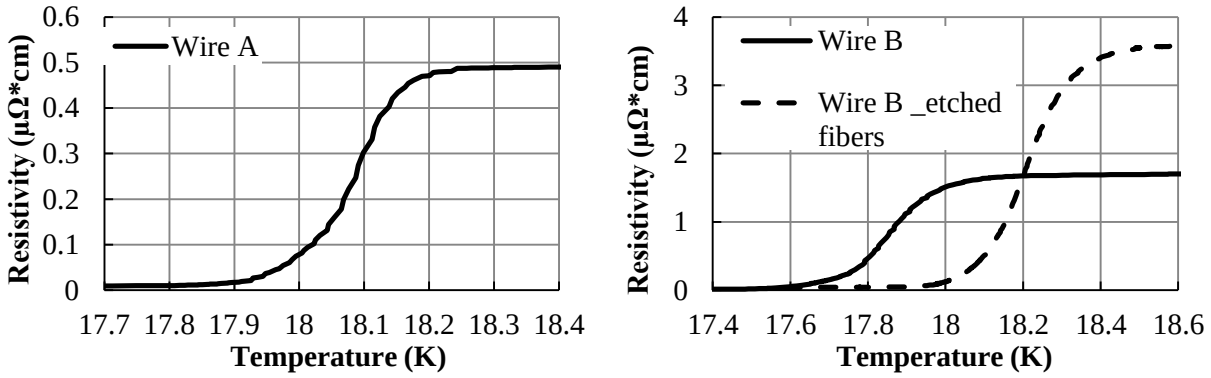


**Figure 5.** The temperature transition of wire A (after removing the Cu stabilization) and wire B - after removing the Cu stabilization and etching out the fibers from bronze matrix

**Table 5.** The critical temperature transition values $T_{0.1}$, $T_{0.5}$ and $T_{0.9}$ taken at resistivity values of 10%, 50% and 90% of the resistivity in the normal state

| Sample | The state of the sample | $T_{c0.9,}$ (K) | $T_{c0.5,}$ (K) | $T_{c0.1,}$(K) | ΔT (K) |
|---|---|---|---|---|---|
| Wire A | Outer copper is removed | 18.20 | 18.10 | 17.96 | 0.24 |
| Wire B | Outer copper is removed | 18.00 | 17.87 | 17.72 | 0.28 |
| | Nb barrier is removed and fibers are etching out from matrix | 18.30 | 18.20 | 18.06 | 0.24 |

It can be seen from the presented results that after the removal of external copper from both wires, the transition temperature of wire A is higher, and the transition width is narrower than that of wire B. The matrix free fibers of wire B show an increase in $T_c$ to extremely high values.

3.5. *The composition of superconducting phase*

The tin content over the cross section of the sub-element (cluster) was carried out by energy dispersive X-ray spectroscopy (EDX). The tin content is determined by at least six lines intersecting sub-elements (clusters) at different angles (figure 6).

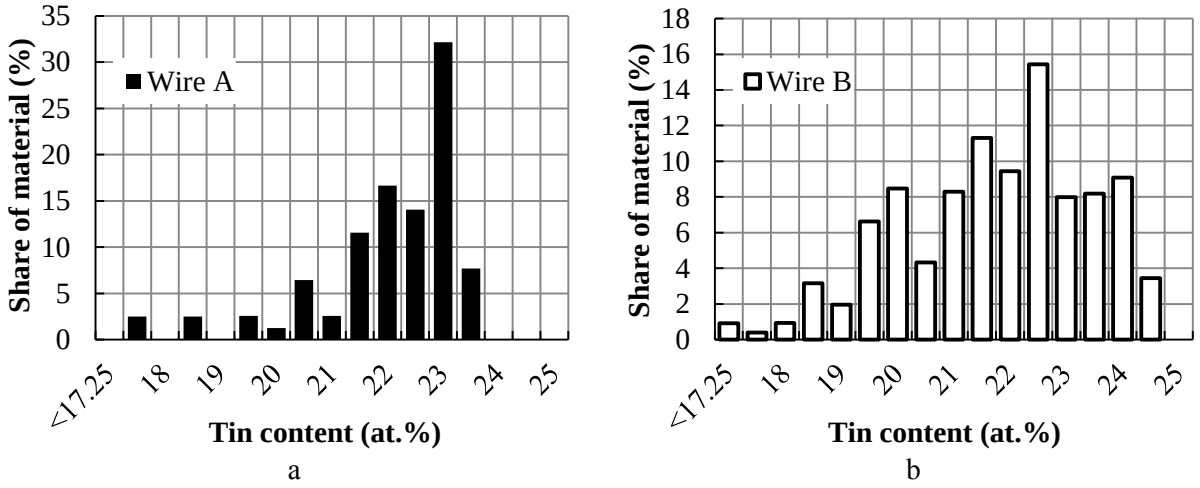


**Figure 6.** Distribution of tin over the cross section of sub-elements (wire A) and clusters (wire B)

It can be seen from figure 6 that the tin distribution gradient in wire B is much larger than in wire A. The tin distribution in wire A is asymmetric with an emphasis on high tin concentrations with a peak in the region of 23.3%. In wire B, the distribution is close to normal with the range of tin content from 18 to 25%, that is in the entire range of the existence of phase A-15.

3.6. *XRD analysis*

Samples of wires A and B for XRD studies were assembled from bundles of wires with a diameter of 3 mm with a polished end. Sample A_powder is made from wire A by completely etching the interfiber copper and then manually grinding it in an agate mortar.

The diffraction patterns of sample of wire A, sample A_powder and sample of wire B are presented in Figure 7. In samples of wire A and B, Cu with an fcc crystal lattice and Nb with a bcc lattice are present, however, the large relative intensity of the maxima of these phases in the sample of wire B indicates a greater amount of Cu and Nb in it. The $Nb_3Sn$ phase is present in both diffraction patterns, but in the sample of wire A its relative amount is noticeably larger. The lines, that are absent in the sample of wire B, but recorded in the diffraction patterns of the wire A, presumably, belong to the phase with the tetragonal crystal lattice $Cu_5Sn_6$.

The results of determining the lattice parameter $a$ and the integral broadening $\beta$ of diffraction peaks (321) are presented in figure 8 and table 6

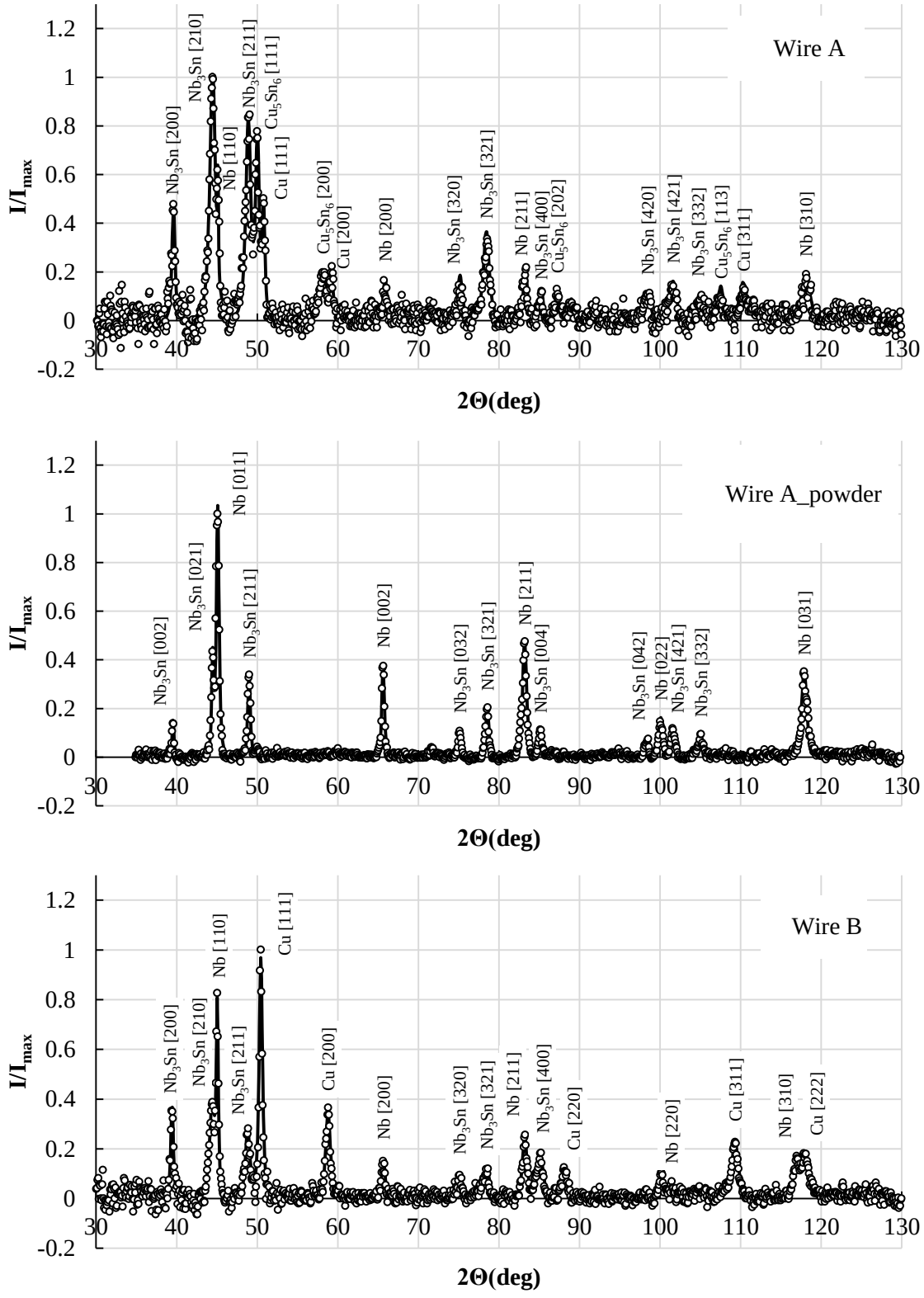


**Figure 7.** X-ray diffraction pattern of wire samples and powder

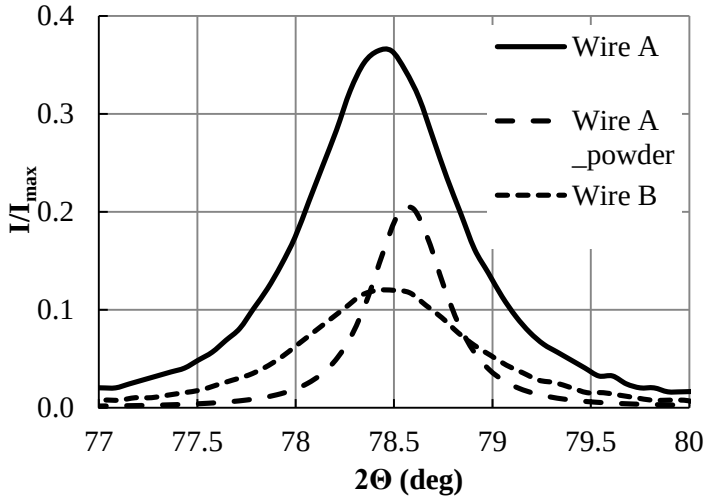


**Figure 8.** Fragments of X-ray diffraction patterns in $Nb_3Sn$(321) direction.

**Table 6.** Lattice parameter and integral broadening of the diffraction peak (321) of the $Nb_3Sn$ phase

| Sample | $a$, Å | $\beta_{321}$, degrees. |
|---|---|---|
| Wire A | 5.2921 | 0.85 |
| A_powder | 5.2871 | 0.44 |
| Wire B | 5.2932 | 0.93 |

## 4. Discussion

Based on the results of comparative tests, it can be concluded that the high current carrying capacity of wire A is determined by a higher level of homogeneity of the superconducting phase composition, which is ascertained by EDX spectroscopy (figure 6). The better homogeneity of the superconducting layer for wire A is also confirmed by higher parameter $n$ (table 3).

The homogeneity of the superconducting phase is determined not only by the composition, but also by the stress state. As it can be seen from figure 5 the transition temperature of wire A is higher, and the transition width is narrower than that of wire B. However, the matrix free fibers of wire B show an increase in $T_c$ to extremely high values (table 5). Based on the data of [6] on the effect of microstresses on the $T_c$-value, it can be assumed that wire B fibers experience significant stress from the bronze matrix and the niobium barrier. The presence of inter-subelement copper in wire A does not provoke such a high stress state, since the value of $T_c$ has a value close to the limiting value, which indicates the presence of a stoichiometric phase with a content of Sn > 23 at.%.

These results are supported by XRD analysis: table 6 shows that the lattice parameter and the broadening of the diffraction peak for wire A are smaller than for wire B, which indicates a more stressed state of the $Nb_3Sn$ phase in the latter.

Moreover, since the powder sample of wire A is crushed and free of copper, and therefore free of internal stresses, the tin content in wire A can be estimated from its lattice parameter. Based on the dependence of the lattice parameter on the tin content from [7], the tin content in wire A is about 23 at.%. This is in agreement with EDX studies (figure 6).

The superconducting phase of wire B, formed under conditions of tin deficiency, has macroinhomogeneity in composition with a tin content from 18 to 25 at.%. The upper critical field reaches $B_K$ = 27.6 T, which is 2 T more than in wire A (figure 2). This indicates the presence of developed diffusion paths of tin in wire B. The results of the $T_c$ determination of sample B before and after the removal of the niobium barrier (figure 5), as well as broadening of diffraction peaks (figure 8), indicate high microstresses in the superconducting layer, which limits its current carrying capacity.

A feature of wire B is the separation of sub-elements into clusters by introducing resistive interlayers of Cu-Mn alloy. The low $D_{eff}$ values relative to $D_{sub\text{-}element}$ on a wire B with a diameter of 1 mm indicates the possibility of suppressing the effect of electromagnetic coupling between clusters (table 4). The effect of dividing a sub-element into clusters is suppressed with decreasing wire diameter to 0.7 mm, which is associated with a distortion of the outer row of sub-elements (figure 1b). Another advantage of wire B compared to wire A is that the design of wire B allows employ reaction heat treatments without duration time limit to increase critical current density without significant deterioration of the RRR parameter (figure 4).

## 5. Conclusion

High current capacity of wires with distributed barriers (wires A) is determined by large volume fraction and high homogeneity of superconducting phase and relatively low level of microstresses. The limiting factor in achieving the critical current density determined by the specification is the electromagnetic interaction between sub-elements. It indicates the insufficiently smooth sub-element geometry and rather thin Cu separators between the sub-elements. The elimination of these disadvantages should lead to an increase in the critical current density and parameter RRR.

The low level of critical current density of wires with common barrier (wires B) is determined by reduced tin concentration which is expressed in macroinhomogeneity and relatively high level of microstresses. The effective diameter $D_{eff}$ reduction of wire B is the result of division of the sub-elements by Cu-Mn separators.

It seems that the wires deformation exceeds the limit at which sub-elements distortion occurs. So the way to increase the performance characteristics is to reduce the initial sub-element dimensions.

Achieving optimal ratios of geometric dimensions without distorting the shape of sub-elements will significantly reduce losses of wire B and increase the performance characteristics.

## 6. Acknowledgment

The authors would like to thank Maria Krylova and the staff of the Resource Center of Electron Microscopy “Nanosonde” at the Research Center “KI” for EDAX analysis, Anastasia Alexandrova (VNIINM) for XRD analysis and Alexey Kalinov (NIITFA) for magnetization measurements.

## References

[1] Ballarino A and Bottura L 2015 *IEEE Trans. Appl. Supercond.***25**(3) 1
[2] Ballarino A, Hopkins S, Bordini B, Richter D, Tommasini D, Bottura L et al. 2019 *IEEE Trans. Appl. Supercond*. **29**(5) 1
[3] Goldfarb R and Itoh K 1994 *J. Appl. Phys.***75**(4) 2115
[4] Ghosh A, Cooley L, Parrell J, Field M, Zhang Y, Hong S 2007 *IEEE Trans. Appl. Supercond*. **17**(2) 2623
[5] Novosilova D, Polikarpova M, Lukyanov P, Krylova M, Tsapleva A, Alekseev M et al. 2018 *Problems of atomic science and technology*. **93**(1) 49
[6] Kozlenkova N, Shikov A, Pantsyrnyi V, Vorobieva A 2002 *Cryogenics* **42**(5) 279
[7] Godeke A 2006 *Supercond. Sci. Technol.* **19**(8) R68